

RF Magnetic Field Profiling with a Dielectric Bore Lining for Traveling Waves in a 3-T MRI Scanner: A Computational Study

Milan M. Ilić^{1,2}, Alexey A. Tonyushkin³, Pranav S. Athalye¹, Nada J. Šekeljić¹,
Andrew J.M. Kiruluta⁴, and Branislav M. Notaroš¹

¹Electrical & Computer Engineering Department, Colorado State University, Fort Collins, CO
milan.ilic@colostate.edu, athalye@rams.colostate.edu, nada.sekeljic@gmail.com, notaros@colostate.edu

²School of Electrical Engineering, University of Belgrade, Serbia
milanilic@etf.bg.ac.rs

³University of Massachusetts Boston, Physics Department, Boston, MA
alexey.tonyushkin@umb.edu

⁴Massachusetts General Hospital, Radiology Department, Boston, MA
kiruluta@physics.harvard.edu

Abstract — Traveling-wave magnetic resonance imaging (MRI) can be advantageous over the classical, quasi-static or near-field MRI. However, it is restricted to ultra-high static magnetic fields in the scanner and the correspondingly high RF excitation magnetic field frequencies due to fundamental constraints in cutoff frequencies of the MRI bore, considered as a waveguide. Through a computational study, we propose translating traveling-wave ideas to a 3-tesla scanner, where the RF magnetic field frequency is 127.8 MHz, using a high-permittivity dielectric layer (lining) that is built into the bore. With the lining, we can achieve traveling-wave modes inside the imaging phantoms even at 3 T, where this is generally not possible. We present results obtained using the higher order method of moments in the surface integral equation formulation, previously established as an efficient, accurate, and reliable technique for modeling of RF fields in MRI applications. Our simulations of a simple circularly polarized RF probe and dielectric lining give rise to a considerably uniform circularly polarized RF magnetic field inside phantoms in the clinical scanner.

Index Terms — 3-tesla MRI, bioelectromagnetics, computational electromagnetics, magnetic resonance imaging, RF coils, RF magnetic field profiling, traveling-wave MRI.

I. INTRODUCTION

In magnetic resonance imaging (MRI), the phenomenon of nuclear magnetic resonance (NMR) is employed in order to extract the imaging information.

In short, the imaging subject is immersed into a strong, static, homogenous magnetic field, \mathbf{B}_0 (e.g., $B_0 = 3$ T in 3-T scanners). This main polarizing field, generated by the main coil, known as the magnet, is axially polarized, i.e., in line with the longitudinal axis (z -axis) of the subject. Consequently, the nuclear magnetic moments of the atoms within the imaging subject (typically Hydrogen atoms) practically align with \mathbf{B}_0 and precess around it at the Larmor frequency f_0 (proportional to B_0). In the plane perpendicular to the z -axis, a circularly polarized RF magnetic field, \mathbf{B}_1 , is then applied in resonance with the precession, i.e., at f_0 , in short pulses. This flips the plane of precession of the nuclei during the pulse duration. By receiving the RF signature emitted during the relaxation of the nuclei, i.e., the return of the precession into the axial direction, the MRI images are generated. For this purpose, a strong, homogeneous, circularly (e.g., right-hand) polarized RF magnetic field \mathbf{B}_1 is highly desirable.

Whereas most MRI machines in human medical practice operate at 1.5 T, state-of-the-art clinical MRI scanners are 3-T systems ($B_0 = 3$ T), i.e., high-field (HF) magnets, with MRI bores measuring typically 60 cm in diameter, which allows full-body human subjects. Advanced clinical centers run 3-T scanners because higher B_0 values yield higher signal-to-noise ratio (SNR), that can be traded for higher spatial resolution, which enables imaging of small details or hard to reach areas inaccessible by 1.5-T scanners, and thus considerably improved diagnostics at 3 T over 1.5 T. However, 3-T scanners are yet far from constituting a majority of MRI machines in hospitals, where 1.5-T

scanners still prevail by a very large margin in part due to higher costs but also due to RF field (\mathbf{B}_1) inhomogeneity issues, specific absorption rate (SAR) constraints, etc.

Indeed, one of the main areas of engineering research in advancing HF MRI scanners is in improving excitors generating RF-excitation magnetic fields, \mathbf{B}_1 , the so-called RF coils at 3 T. For 3-T clinical, preclinical, and research MRI scanners, the RF coils are mostly birdcage coils [1]. Recent developments aimed at improving \mathbf{B}_1 field uniformity of body coils in preclinical scanners at 3 T include various modifications of the birdcage coil, such as a birdcage coil with detached endcaps [2], TEM coils [3-5], and spiral coils [6]. Birdcage coils and their variants are, however, designed as close-range or near-field volume coils.

Traveling-wave (TW) magnetic resonance imaging (MRI), unlike a near-field MRI, functions by using the MRI scanner bore as a waveguide in which desired traveling-wave modes are excited. However, TW MRI is primarily reserved for ultra-high-field (UHF) systems, i.e., for MRI scanners with $B_0 > 4$ T, due to fundamental constraints in cutoff frequencies of TW inside hollow waveguides [7]. In 3-T systems, the Larmor frequency, and the frequency of the \mathbf{B}_1 field, is $f_0 = 127.8$ MHz [8]. This falls considerably below the cutoff frequency of the bore considered as a cylindrical waveguide, even when loaded with a human body. On the other hand, the potential benefits of TW MRI include large field of view (FOV) coverage, robust RF sources, field profile engineering with a variety of available modes, and a more comfortable open environment. Some of the promising developments for UHF TW MRI are multichannel probes or patch antennas [9], helical-antenna RF coils [10], dielectric linings [11], and metabores [12]. At clinical strengths, as the bore becomes wider, it is important to design a homogeneous RF field profile without compromising patient's comfort. Here we propose translating TW MRI ideas to 3-T scanners using a specially designed high-permittivity dielectric layer built into the bore. The TW with dielectric lining may complement a body RF coil inside wide-bore clinical scanners.

II. METHOD AND MATERIALS

For our computational study, we used the higher order method of moments (MoM) in the surface integral equation (SIE) formulation [13,14]. Previously, we had thoroughly verified and validated the higher-order MoM-SIE technique in modeling of RF fields in MRI applications in both HF and UHF MRI regimes by comparisons against two well-established commercial full-wave computational electromagnetics codes [8, 10, 15, 16]. These are a MoM code WIPL-D and a finite element method (FEM) code ANSYS HFSS. The simulations setup of concentric and coaxial three-layers

metallic waveguide ($D = 60$ cm) is shown in Fig. 1. The MRI bore is lined with a layer of dielectric from the inside with thickness $T_D = 5$ cm. The dielectric layer (lining) consists of high-permittivity material with $\epsilon_r = 132$, $\mu_r = 1$, $\sigma = 0.03$ S/m. To investigate RF field profiling, we carried out our simulations with two phantoms of different geometries. The first phantom is a saline-filled uniform cylinder ($L = 1$ m, $D = 15$ cm, $\epsilon_r = 81$, $\sigma = 0.6$ S/m), as shown in Fig. 1 (a). To eliminate a standing wave, the phantom has an additional saline-filled buffer at the far end of the bore of length $L_C = 40$ cm. The second phantom is a human body model filled uniformly with saline solution ($\epsilon_r = 81$, $\sigma = 0.6$ S/m), as depicted in Fig. 1 (b). To excite RF fields inside the phantoms, we used a pair of capacitively loaded Tx/Rx loop-coils in orthogonal arrangement, Fig. 1 (c), driven in quadrature that are capable of generating circularly polarized (CP) RF field (needed for MRI) inside the bore [17]. The center of the loops is located at the opening of the bore, Fig. 1 (a).

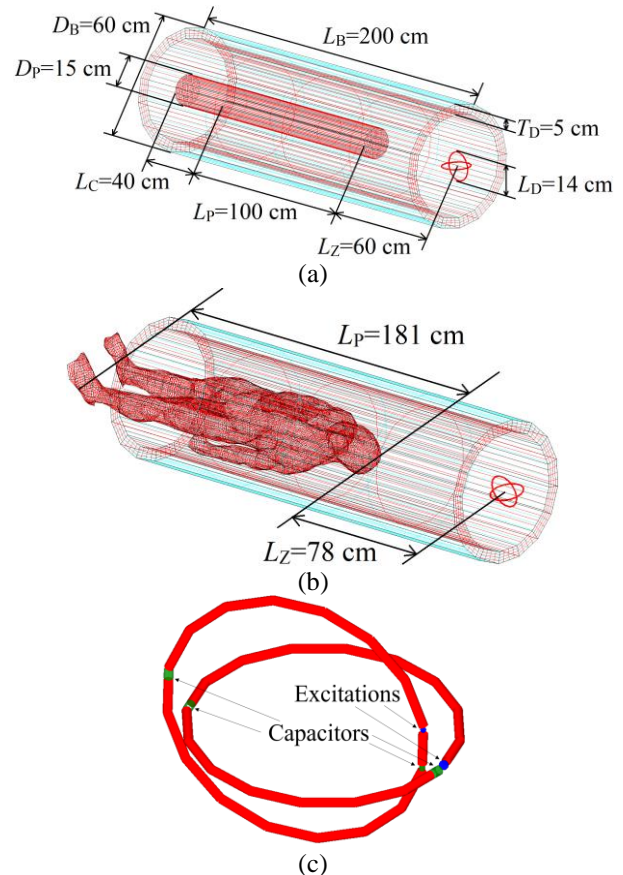


Fig. 1. Simulations setup of lossy-dielectric (saline) phantoms inside a 3-T MRI bore with a dielectric layer (lining): (a) cylindrical phantom; (b) human body phantom; and (c) orthogonal capacitively loaded Tx/Rx loop-coils excited in quadrature, to achieve circular polarization of the magnetic field along the bore axis.

III. RESULTS AND DISCUSSION

The simulations of RF magnetic field (B_1) profiles inside the dielectric cylindrical phantom in the 3-T bore [Fig. 1 (a)] without and with the dielectric lining are shown in Figs. 2 and 3–4, respectively. Note that the scale for B values is adopted to be the same in all graphs in Figs. 2–4, for ease of reference and comparison. With this, the maximum value of 1 nT in the graphs is certainly not optimal (it is too high) for the graphs in Fig. 2 individually, but it enables direct visual comparison of B field intensities between the two distinct cases considered, the structure without and with the dielectric lining, so between the respective graphs in Figs. 2 and 3–4. Figures 2 (a)–(b) and 3 depict the right-hand CP (RCP) RF magnetic field, usually denoted as B_1^+ , propagating inside the phantom without and with the lining, respectively, in coronal and axial planes. The longitudinal field profile with the lining, in Fig. 4 (a), produces a slight bump at the entrance of the phantom but stabilizes at a relatively constant initial value. Both longitudinal and transverse profiles, in Figs. 4 (a) and (b), show a very predominant RCP component of the transverse \mathbf{B}_1 , B_1^+ , over the left-hand CP (LCP) component, B_1^- , and hence an excellent B_1^+/B_1^- ratio, desirable for MRI.

From Figs. 2 (a)–(b), the B_1^+ field inside the phantom without dielectric lining is of very low intensity, particularly when compared with the same field when the lining is inserted in the structure, in Figs. 3–4. Also, it produces unfavorable rapid decay along the z -axis, Fig. 2 (c), dropping significantly after distance of $z = 0.25$ m. On the other hand, the same field with the lining, as can be observed from Figs. 3 (a)–(b) and 4 (a), shows excellent propagation along the bore and maintains above one half of its peak strength in the longitudinal plots throughout the entire phantom. In addition, in the bore with the lining (Figs. 3–4) the same field is much stronger, i.e., it is about five times stronger around the peak strength in the longitudinal plot in Fig. 4 (a) than in Fig. 2 (c) (with the same excitation in both figures) and about eight times stronger around the peak strength in the axial cross section at $z = 0.15$ m. This difference increases even further into the phantom where at the center of the phantom the peak strength is about 30 times stronger when the dielectric lining is used. Moreover, the field profile in the axial cross section in Fig. 4 (b) shows symmetric and relatively lower B_1^- , component than in Fig. 2 (d), indicating better B_1^+/B_1^- ratio in the right hand side of the figure. Finally, we note that stronger, non-decaying, and more uniform B_1^+ , as well as better B_1^+/B_1^- ratio, in all cross sections in Figs. 3–4 than those in Fig. 2, will ultimately lead to better SNR in the

MRI image [1] in the bore with the dielectric lining. Unmodified 3-T scanner may allow propagating TW modes in larger phantoms with appropriate excitations. However, we here choose the parameters (narrow diameter of the cylinder and long distance $L_Z = 60$ cm from the probe) that normally do not support TW.

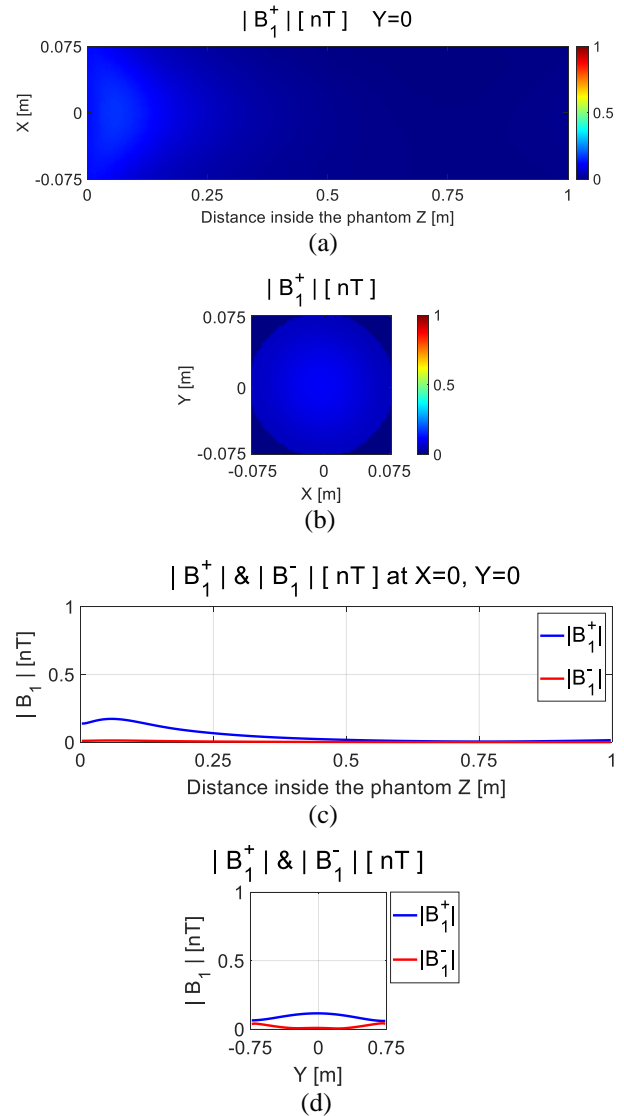


Fig. 2. Simulations of B_1 field in the cylindrical saline phantom in the MRI bore at 3 T [Fig. 1 (a)] without dielectric layer: (a) 2-D B_1^+ field profile in central coronal plane; (b) B_1^+ profile in axial plane at $z = 0.15$ m; (c) B_1^+ (blue) and B_1^- (red) longitudinal field distributions; and (d) transverse field distributions. The scale for B values is adopted to be the same (maximum value 1 nT) as in Figs. 3 and 4 (on the next page), for easier comparison.

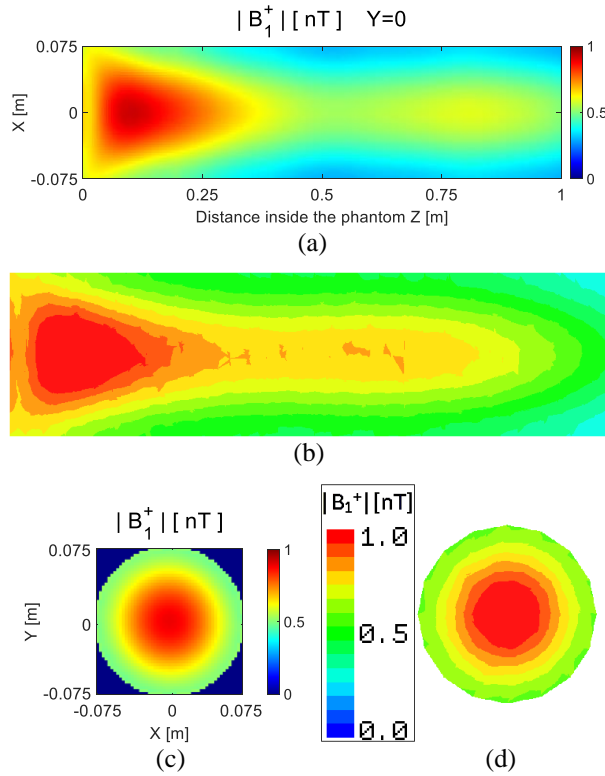


Fig. 3. 2-D B_1^+ field profiles in the cylindrical saline phantom for the MRI bore with dielectric lining as in Fig. 1 (a), to be compared with Figs. 2 (a)–(b): (a) MoM-SIE results for the central coronal plane; (b) ANSYS HFSS (FEM) solution in the coronal plane; (c) MoM-SIE simulation for the axial plane at $z = 0.15$ m; and (d) HFSS results in the axial plane.

The MoM-SIE simulation model with the cylindrical phantom without the dielectric lining employed 800 elements with 2,640 unknowns and the simulation time was 20.95 seconds. The model with the cylindrical phantom with the dielectric lining had 5,808 elements which yielded 14,416 unknowns and the simulation time was 224.34 seconds. The simulations were run on a desktop computer with Intel i7-3770 CPU (3.4 GHz) and 16 GB RAM. In addition, we show in Figs. 3 (b) and (d) the results obtained by ANSYS HFSS, and an excellent agreement between the MoM-SIE [Figs. 3 (a) and (c)] and HFSS solutions is observed (having in mind the differences of the color maps and unavoidable mesh imprints). Note that the two solution approaches used for comparison are completely different, both conceptually and numerically; the MoM-SIE is a surface modeling technique that solves boundary integral equations for currents, while HFSS is a

volumetric modeling technique that solves partial differential equations for fields.

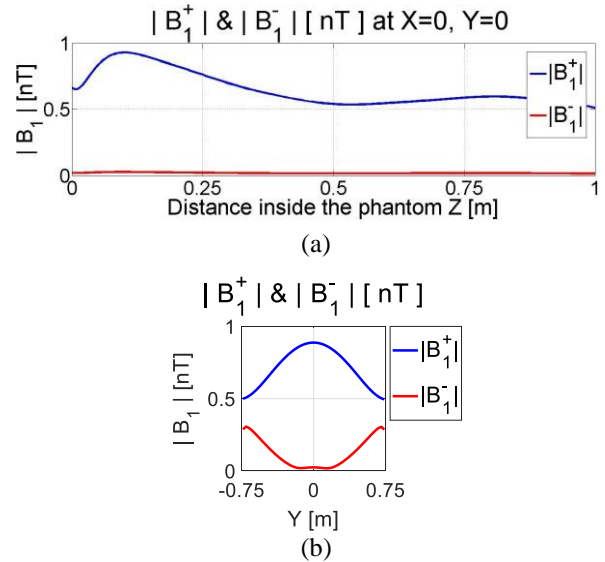


Fig. 4. B_1^+ and B_1^- field distributions for the MRI bore with dielectric lining [Fig. 1 (a)] in (a) longitudinal and (b) transverse directions, for comparison with Figs. 2 (c)–(d).

We extended our simulations to a human body model uniformly filled with saline [Fig. 1 (b)], and the results are given in Figs. 5 and 6 for the bore without and with the dielectric lining, respectively. Overall, we observe a pattern similar to the cylindrical phantom along the human body phantom with the dielectric lining bore (Fig. 6) and rapid decay without lining (Fig. 5).

It can also be concluded from Figs. 5 and 6 that the dielectric lining significantly improves the B_1^+ strength as well as the B_1^+/B_1^- ratio within the imaging subject with all associated benefits already discussed in the first example. The lower B_1^+ at the shoulders corresponds to the Gaussian field profile of the dielectric-lining bore. The MoM-SIE simulations of the structure with the human body phantom model involved 1,566 elements and 6,112 unknowns without the dielectric lining, and simulation time was 220.24 seconds. When the dielectric lining was added, these parameters increased to 2,798 elements, 14,432 unknowns, and 377.92 seconds. Further optimizations of the field profile may include higher dielectric constant material for the lining as well as non-uniform permittivity ϵ_r along the z -coordinate to compensate for the drop of the field in various body regions, such as the neck. Similar effects, qualitatively, can be achieved using dielectric pads [18] or collars [8].

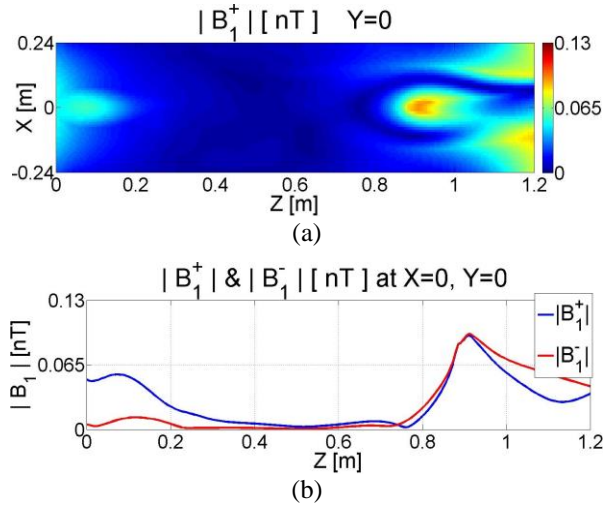


Fig. 5. Simulations of the human body model phantom in the MRI bore at 3 T [Fig. 1 (b)] without dielectric liner: (a) B_1^+ in coronal plane; (b) B_1^+ (blue) and B_1^- (red) profiles along the z -coordinate, inside the phantom. The RF coils are located at the opening of the bore (head side); the head of the phantom is at the isocenter, so the lower part of the body is outside of the bore ($z > 1.2$ m).

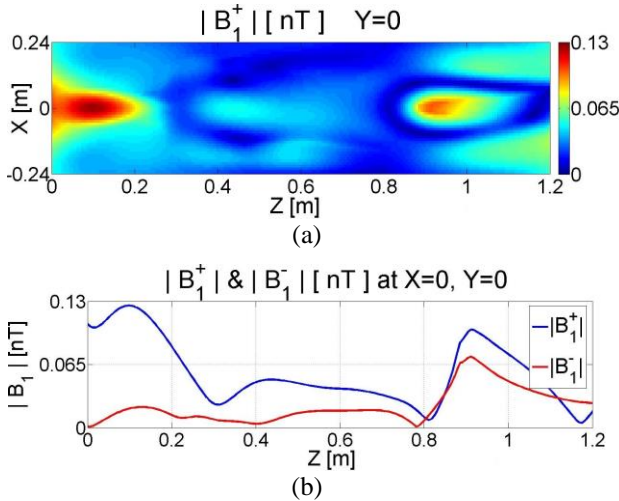


Fig. 6. The same as in Fig. 5 but for the MRI bore with dielectric lining as in Fig. 1 (b).

In terms of realizability and implementation, high-permittivity materials are more available (as opposed to metamaterials, like negative ϵ and negative μ , and double negative metamaterials, as well as most other metamaterials suggested for lower-field TW MRI [19]). They are widely used in dielectric resonators based on BaTiO_3 compounds, where ϵ_r can be up to 300. Other realizations are possible as well.

IV. CONCLUSIONS

This paper has proposed translating traveling-wave ideas to a 3-T scanner, where the RF magnetic field frequency is considerably below the cutoff frequency of the bore, using a high-permittivity dielectric lining built into the bore. Our simulation model with a dielectric layer and a simple circularly polarized RF probe gives rise to a relatively uniform TW with an excellent RCP/LCP field ratio inside the phantom in the 3-T clinical scanner. The dielectric lining could be incorporated into the wide bore to shape the B_1 field profile from the body RF coil or for TW MRI at lower B_0 fields. Future work will include optimization of dielectric lining parameters and investigation of the impact of a non-uniform layer on a heterogeneous human body model.

ACKNOWLEDGEMENT

This work was supported by the National Science Foundation under grants ECCS-1307863 and ECCS-1810492.

REFERENCES

- [1] C. E. Hayes, W. A. Edelstein, J. F. Schenck, O. M. Mueller, and M. Eash, "An efficient, highly homogeneous radiofrequency coil for whole-body Nmr imaging at 1.5-T," *J Magn Reson.*, vol. 63, no. 3, pp. 622-8, 1985.
- [2] M. Alecci, C. M. Collins, J. Wilson, W. Liu, M. B. Smith, and P. Jezzard, "Theoretical and experimental evaluation of detached endcaps for 3 T birdcage coils," *Magn Reson Med.*, vol. 49, pp. 363-370, 2003.
- [3] J. T. Vaughan, G. Adriany, C. J. Snyder, J. Tian, T. Thiel, L. Bolinger, H. Liu, L. DelaBarre, and K. Ugurbil, "Efficient high-frequency body coil for high-field MRI," *Magnetic Resonance in Medicine: Official Journal of the Society of Magnetic Resonance in Medicine/Society of Magnetic Resonance in Medicine*, vol. 52, no. 4, pp. 851-859, 2014.
- [4] C. A. Van den Berg, B. Van den Bergen, J. B. Van de Kamer, B. W. Raaymakers, H. Kroeze, L. W. Bartels, and J. J. W. Lagendijk, "Simultaneous B+ homogenization and specific absorption rate hotspot suppression using a magnetic resonance phased array transmit coil," *Magn Reson Med.*, vol. 57, pp. 577-586, 2007.
- [5] J. Tian, L. DelaBarre, J. Strupp, J. Zhang, J. Pfeuffer, M. Hamm, J. Nistler, and K. Ugurbil, "Searching for the optimal body coil design for 3T MRI," *Proceedings of the 21st Annual Meeting, International Society for Magnetic Resonance in Medicine*, Salt Lake City, Utah, USA, pp. 2746,